Biosensors and Bioelectronics 74 (2015) 291–298

Contents lists available at ScienceDirect

Biosensors and Bioelectronics

journal homepage: www.elsevier.com/locate/bios

Carbohydrate derivative-functionalized biosensing toward highly sensitive electrochemical detection of cell surface glycan expression as cancer biomarker

Xinai Zhang [a,*], Wenjie Lu [b], Jianzhong Shen [a], Yuxiang Jiang [a], En Han [a], Xiaoya Dong [a], Jiali Huang [a]

[a] School of Food and Biological Engineering, Jiangsu University, Zhenjiang 212013, PR China
[b] School of Energy and Power Engineering, Jiangsu University, Zhenjiang 212013, PR China

ARTICLE INFO

Article history:
Received 16 May 2015
Received in revised form
16 June 2015
Accepted 19 June 2015
Available online 28 June 2015

Keywords:
Glycan expression
Cancer biomarker
Carbohydrate derivative
Electrochemical biosensor
Signal amplification

ABSTRACT

Accurate and highly sensitive detection of glycan expression on cell surface is extremely important for cancer diagnosis and therapy. Herein, a carbohydrate derivative-functionalized biosensor was developed for electrochemical detection of the expression level of cell surface glycan (mannose used as model). Thiomannosyl dimer was synthesized to design the thiomannosyl-functionalized biosensor by direct and rapid one-step protocols. The biosensing surface-confined mannose could effectively mimic the presentation of cell surface mannose and was responsible for competing with mannose on cancer cells in incubation solution. Greatly enhanced sensitivity was achieved by exploiting the excellent conductivity of multiwalled carbon nanotube/Au nanoparticle (MWNT/AuNP), the amplification effect of MWNTs, and the favorable catalytic ability of horseradish peroxidase (HRP). Using competitive strategy, the developed biosensor exhibits attractive performances for the analysis of mannose expression with rapid response, high sensitivity and accuracy, and possesses great promise for evaluation of cell surface glycan expression by using a greater variety of lectins.

1. Introduction

Glycans, the key components of cell surface glycolipids and glycoproteins, play critical roles in fundamental biological events including bacterial pathogenesis, inflammation, and cancer cell metastasis (Ohtsubo and Marth, 2006; Helenius and Aebi, 2001; Haslam et al., 2006; Zhang et al., 2011; Matsumoto et al., 2009). According to research, the expression levels of glycans can be acted as therapeutic targets or clinical biomarkers to convey information about the physiological state of cells (Ding et al., 2009; Zhang et al., 2010; Hollingsworth and Swanson, 2004; Gorelik et al., 2001). Therefore, it is urgent to develop simple technology for sensitive and accurate assay of glycan expression on cell surface.

Consequently, many kinds of biosensors were developed for glycan analysis based on optical, electrochemical, and piezoelectric transducers (Park et al., 2009; Dai et al., 2006; Lyu et al., 2008; Svarovsky and Joshi, 2014). Among them, electrochemical biosensors have been well recognized to be a promising solution for signal transduction due to the fact that electrochemical detectors are simple, portable and inexpensive (Zhang et al., 2009; Peng et al., 2014; Zheng et al., 2014). Combining with nanotechnology in materials science, electrochemical biosensor opens up new horizons for the highly sensitive determination of biological and environmental analytes because of the nanomaterial-based signal amplification platform (Zhang et al., 2014; Ma and Nakazato, 2014). For example, a high sensitive biosensor based on FePt/CNTs nanocomposite/N-(4-hydroxyphenyl)-3,5-dinitrobenzamide modified carbon paste electrode was developed for simultaneous determination of glutathione and piroxicam (Karimi-Maleh et al., 2014). The 2,2′-[1,2-ethanediylbis(nitriloethylidyne)]-bis-hydroquinone double-wall carbon nanotube paste electrode was reported for simultaneous determination of epinephrine, uric acid and folic acid (Beitollahi et al., 2008). A highly sensitive nanostructure-based electrochemical sensor was described for electrocatalytic determination of norepinephrine in the presence of acetaminophen and tryptophan (Mazloum-Ardakani et al., 2011). Carbon paste electrode modified with cobalt porphyrin and TiO_2 nanoparticles was used for the determination of levodopa in the presence of carbidopa (Mazloum-Ardakani et al., 2012).

However, regarding the assay of cell surface glycans, many researchers are enthusiastic in looking for effective ways to improve

* Corresponding author. Fax: +86 511 88780201.
E-mail address: zhangxinai@mail.ujs.edu.cn (X. Zhang).

http://dx.doi.org/10.1016/j.bios.2015.06.051
0956-5663/

the analysis performance due to the lack of electroactive groups in glycans. In this respect, various methods based on labeling technologies with electroactive moieties, enzymes, interactive substances, and nanomaterials have been developed to enhance the electrochemical signal (Singh et al., 2013; Zhang et al., 2015; Lotierzo et al., 2012; Scavetta et al., 2014). Among these labels, enzymes have attracted broad attentions because of their easy labeling and especially signal amplification for sensitivity enhancement (Zhao et al., 2014; Jeong et al., 2013).

With the aim of designing a successful biosensor, the applied biomaterials for sensing interface are crucial for improving biosensor performance. Inspired by the concept of DNA and protein biosensors, carbohydrate-functionalized biosensors, which are composed of carbohydrate attached to a solid surface, have recently been developed as reliable and efficient tools for the assay of biological analytes (Pussak et al., 2013; Shin et al., 2005; Martin et al., 2013). This technology not only facilitates fast and sensitive analysis of a large number of biomolecules, but also effectively mimics the presentation of glycans on living cell surface to exhibit multivalent interactions with receptors (Bian et al., 2014; Mader et al., 2012). Regarding the construction of the carbohydrate-functionalized biosensor, the efficient immobilization of carbohydrates is an important factor because carbohydrates do not have functional groups (Yamada et al., 2013). Most of the attempted strategies for carbohydrate immobilization so far rely on multistep protocols aimed at indirect immobilization. However, the utilization of these methods might be hindered owing to the biosensor requirement for one-step protocols with direct and rapid immobilization (Seo et al., 2007). Alternatively, the development of carbohydrate derivatives containing anchor groups (e.g., thiols, disulfides, amines, selenols) to functionalize electrode surfaces provides a simple and rapid avenue for the biosensor preparation (Zou et al., 2008; Deng et al., 2011).

In this work, an amplified carbohydrate derivative-functionalized electrochemical biosensor was developed for competitive assay of glycan expression on living cancer cells. Here, mannose present on cancer cells derived from human lung, liver, and prostate was used as a model glycan. A thiol-derivatized carbohydrate (thiomannosyl dimer, $[\text{mannose–S}]_2$), comprising of disulfide portion [S–S] and mannose portion, was synthesized to design the biosensor by direct and rapid one-step protocols, in which the disulfide part anchored the molecule and the mannose portion was responsible for competing with glycan on cell surface. The multiwalled carbon nanotube/Au nanoparticle (MWNT/AuNP)-modified glassy carbon electrode (GCE) was used as substrate to construct the thiomannosyl-functionalized biosensor (GCE/MWNT/Au–S–mannose). Owing to the large surface area and excellent conductivity of MWNT/AuNP, the substrate not only provided a highly suitable environment for thiomannosyl dimer assembling through Au–S bond but also played a significant role in signal enhancement. The {Con A–MWNT–HRP} bioconjugates, as recognition elements, were fabricated by exploiting the amplification effect of MWNTs for loading enormous horseradish peroxidase (HRP) labels and mannose-specific concanavalin A (Con A) (Fig. 1a). Unlike the two-step sandwich analysis, the present protocol relied on a rapid and one-step competitive assay, in which the biosensing surface-confined mannose competed with cell surface mannose to recognize the {Con A–MWNT–HRP} bioconjugates by the specific interaction between mannose and Con A. The analysis of cell surface mannose was performed based on the catalytic reaction of HRP toward the oxidation of hydroquinone (QH_2) by H_2O_2, which could introduce further signal enhancement (Fig. 1b). Under optimal conditions, the proposed biosensor exhibited attractive performances for the analysis of cancer cells with wide linear ranges and low detection limits. The average amount of mannose on single cell surface was also evaluated to be 1.3×10^{10} molecules for QGY-7703 (liver cancer cell), 5.8×10^{10} molecules for A549 (lung cancer cell), and 1.9×10^{10} molecules for LNCaP (prostate cancer cell). Therefore, the carbohydrate derivative-functionalized electrochemical biosensor gives a useful protocol for glycan assay with high sensitivity, accuracy and rapid response, and may help the medical diagnosis and treatment in the early process of cancer.

2. Experimental

2.1. Reagents and materials

Concanavalin A (Con A), horseradish peroxidase (HRP, MW

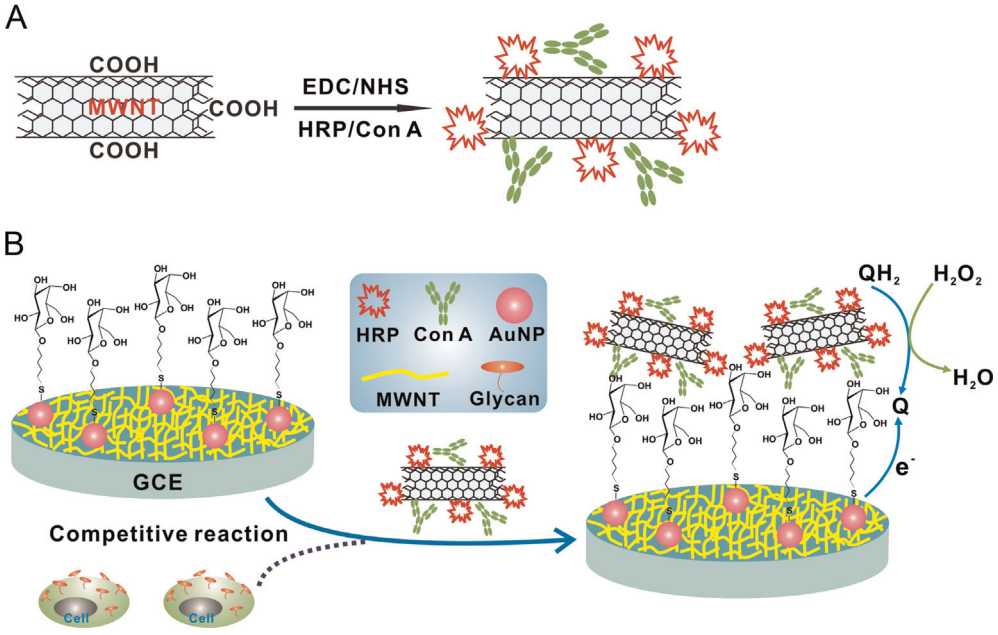

Fig. 1. Schematic illustration of (a) the preparation of the {Con A–MWNT–HRP} bioconjugates and (b) the thiomannosyl-functionalized electrochemical biosensor for competitive assay of mannose expression on cancer cells.

44,000), HRP-labeled Con A ({Con A–HRP}), 1-ethyl-3-(3-dimethylaminopropyl) carbodiimide (EDC) and N-Hydroxysuccinimide (NHS) were purchased from Sigma-Aldrich (St. Louis, MO, USA). Fluorescein Con A was obtained from Vector Laboratories (Burlingame, CA, USA). Multiwalled carbon nanotubes (MWNTs, 10–30 nm in diameter) were obtained from Nanotech Port Co., Ltd. (Shenzhen, China). Mannose was purchased from Aladdin Reagent Database Inc. (Shanghai, China). Gold chloride tetrahydrate ($HAuCl_4 \cdot 4H_2O$), H_2O_2, hydroquinone (QH_2), N,N-dimethylformamide (DMF), Tris–HCl buffer (pH 7.4), Tween-20 and other chemical reagents were obtained from Chemical Reagents Co., Ltd. (Shanghai, China). All solutions were prepared with MilliQ water (18 MΩ cm) from a Millipore system.

2.2. Cell culture and treatment

Human liver cancer cell: QGY-7703, lung cancer cell: A549, and prostate cancer cell: LNCaP, were obtained from Institute of Biomedical Sciences, East China Normal University (Shanghai, China). These three cancer cells were maintained in RPMI-1640 Medium with 10% fetal bovine serum at 37 °C in a humidified atmosphere of 5.0% CO_2. All cell culture reagents were from Sigma-Aldrich (St. Louis, MO, U.S.A.). At the logarithmic growth phase, cells were trypsinized and washed twice with phosphate-buffered saline (PBS, pH 7.4) by centrifugation at 1000 rpm for 5 min. The sediment was dispersed in Tris–HCl buffer (pH 7.4, containing 1.0 mM Mn^{2+}, 1.0 mM Ca^{2+} and 0.10 M Na^{+}) to obtain a homogeneous cell suspension.

2.3. Apparatus

All electrochemical measurements were performed with a CHI 660C workstation (CH Instruments Inc., Austin, TX, USA). A conventional three-electrode configuration was employed all through the experiment, which involved a glassy carbon working electrode (GCE), a platinum wire auxiliary electrode, and a saturated calomel reference electrode (SCE) (Chenhua Instruments, Shanghai, China). Electrochemical impedance spectroscopy (EIS) was carried out within frequency range of 0.10 Hz to 100 kHz at amplitude of 5 mV, cyclic voltammetry (CV) at a scan rate of 100 mV s^{-1}, and amperometric measurement in a stirred cell by applying a potential of −0.06 V to the working electrode. Transmission electron microscopy (TEM) was collected on JEM-2100 (JEOL Ltd., Tokyo, Japan). Scanning electron microscopy (SEM) was carried out on S-4800 (Hitachi Co., Ltd., Tokyo, Japan). UV–vis absorption spectra were recorded on a Cary 500 UV–vis–NIR spectrometer (Varian Inc., Palo Alto, CA, USA). Fourier transform infrared (FT-IR) spectra were recorded on a Nicolet Nexus 670 instrument (Thermo Nicolet Co., USA) in KBr pellet form. Fluorescence images were collected by fluorescence microscope (Leica DM4000B, Leica Microsystems, Nussloch, Germany).

2.4. Preparation of the {Con A–MWNT–HRP} bioconjugates

The {Con A–MWNT–HRP} bioconjugates were prepared by exploiting the amplification effect of MWNTs as carriers for loading enormous Con A and HRP, and the preparation process was described in Fig. 1a. Briefly, MWNTs were first purified by refluxing in 3.0 M HNO_3 for 24 h. The purified MWNTs were chemically shortened by sonication in a mixture (1:3 v/v) of concentrated HNO_3 (70%) and H_2SO_4 (98%) for 5 h at 70 °C by a 100 W ultrasonic cleaner. The dispersion was filtered and washed repeatedly with water until pH was ~7.0, and then the resulting MWNTs were dried under vacuum overnight. Subsequently, MWNTs were redispersed in PBS by sonication to give a black dispersion (1.0 mg mL^{-1}). This dispersion was mixed with a 10 mL portion of EDC (400 mM) and NHS (100 mM) solution, and stirred at room temperature (RT) for 30 min. The mixture was centrifuged at 15,000 rpm for 5 min to obtain the precipitate of carboxyl-activated MWNTs. The precipitate was washed with water three times, and then redispersed in PBS (4.0 mL). The MWNT solution was incubated with Con A (1.0 mg mL^{-1}) and HRP (20 mg mL^{-1}) overnight at RT under shaking to prepare the {Con A–MWNT–HRP} bioconjugates. The bioconjugates were isolated by centrifugation at 5000 rpm for 10 min and washed twice with PBS to remove free Con A and HRP. After that, 0.05% Tween-20/Tris–HCl buffer (2.0 mL) was added to the prepared bioconjugates to form a homogeneous dispersion and stored in refrigerator at 4 °C.

2.5. Preparation of the thiomannosyl-functionalized biosensor

In the case of the biosensor design, GCE/MWNT/AuNP was used as a substrate for thiomannosyl dimer assembling through Au–S bond, which was fabricated by first introduction of MWNTs on GCE (3 mm in diameter) surface and then electrodeposition of AuNPs by multi-potential step. First, GCE was polished to a mirror using 0.05 μm alumina on a polishing micro-cloth followed by rinsing with pure water prior to surface modification. After successive sonication in acetone, HNO_3 (1:1 v/v), NaOH (50% w/w) and water, the clean GCE surface was modified by casting MWNTs in DMF (10 μL, 0.10 mg mL^{-1}) and dried under infrared lamp. Subsequently, AuNPs were electrodeposited onto the MWNT-modified GCE via multi-potential step from +1.055 to −0.045 V vs SCE for 15 s in H_2SO_4 (0.50 M) solution containing $HAuCl_4$ (0.10 mM) (Dai et al., 2004). The GCE/MWNT/AuNP was incubated with thiomannosyl dimer (10 mg mL^{-1}, which was prepared according to the previous paper (Zhang et al., 2011)) in anhydrous ethanol overnight at 4 °C. The electrode was washed with ethanol and water, and then dried under nitrogen to give the thiomannosyl-functionalized biosensor.

2.6. Enzyme-amplified electrochemical detection

The thiomannosyl-functionalized biosensor was incubated with a mixture of the {Con A–MWNT–HRP} bioconjugates (0.20 μM) and cancer cells at a given concentration for 60 min at RT, and then the biosensing surface-confined mannose competed effectively with cell surface mannose to specifically recognize the bioconjugates (Fig. 1b). After the competitive reaction, the resulting electrode was washed thoroughly with PBS to minimize the background response. The electrochemical measurement was performed in degassed PBS (0.10 M, pH 7.4) containing H_2O_2 (0.80 mM) and QH_2 (0.20 mM). HRP in the bound bioconjugates on the biosensing surface could catalyze the oxidation of QH_2 by H_2O_2 and the enzymatic product was finally recorded by differential pulse voltammetry (DPV) measurements to obtain a reduction signal. The DPV measurements were from +0.60 to −0.60 V with pulse amplitude of 50 mV and width of 50 ms. With an increasing cell concentration, a decreased peak current was obtained and a strategy for analysis of cancer cells and mannose expression on cell surface was established by the decrease of peak current.

3. Results and discussion

3.1. Characterization of the thiomannosyl-functionalized biosensor

SEM was used to charapcterize GCE modified with MWNT, MWNT/AuNP and MWNT/Au–S–mannose, respectively. MWNTs were mostly in the form of small bundles or single tubes on GCE (Fig. 2a). The well-dispersed AuNPs (white dots) decorated on the walls of nanotubes quite uniformly (Fig. 2b). The uniform

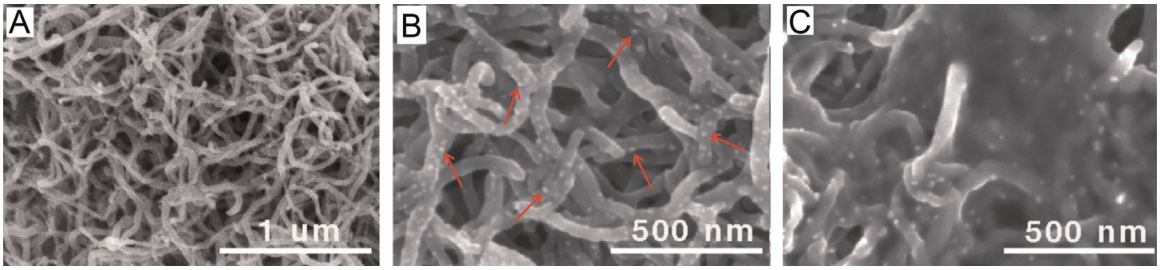

Fig. 2. Scanning electron microscopy (SEM) images of (a) GCE/MWNT, (b) GCE/MWNT/AuNP (Au NPs (white dots) decorated uniformly on the walls of MWNTs and six particles of them are shown with arrows), and (c) GCE/MWNT/Au–S–mannose.

nanostructure possessed the advantages of high surface area, good mechanical stability and enhanced conductivity, and thus provided a highly suitable environment for thiomannosyl dimer assembling by direct and rapid one-step protocols. The surface of the thiomannosyl-functionalized biosensor became much rougher and richer in texture (Fig. 2c).

The electrochemical properties of the thiomannosyl-functionalized biosensor were studied by EIS. Fig. S1A (Supplementary) illustrates the Nyquist plots of EIS for the different modified electrodes in the presence of redox probe $Fe(CN)_6^{3-/4-}$. At a bare GCE, the redox process of the probe showed an electron-transfer resistance (R_{et}) of about 240 Ω (curve a). When MWNTs were modified on the electrode surface, the R_{et} decreased significantly (curve b). The electrodeposition of AuNPs on the MWNT-modified GCE further facilitated the electron transfer, exhibiting an almost straight line (curve c). It was reasonable that MWNTs and AuNPs could increase the effective surface area and accelerate electron transfer. Subsequently, thiomannosyl dimer was assembled on GCE/MWNT/AuNP (curve d), which partially blocked the electron transfer of the redox probe and resulted in an obvious increase of R_{et}. CVs also confirmed the electrical communication between the redox probe $Fe(CN)_6^{3-/4-}$ and the electrodes upon the stepwise modification process (Supplementary Fig. S1B). The obtained results from the CVs were in good accordance with those from EIS.

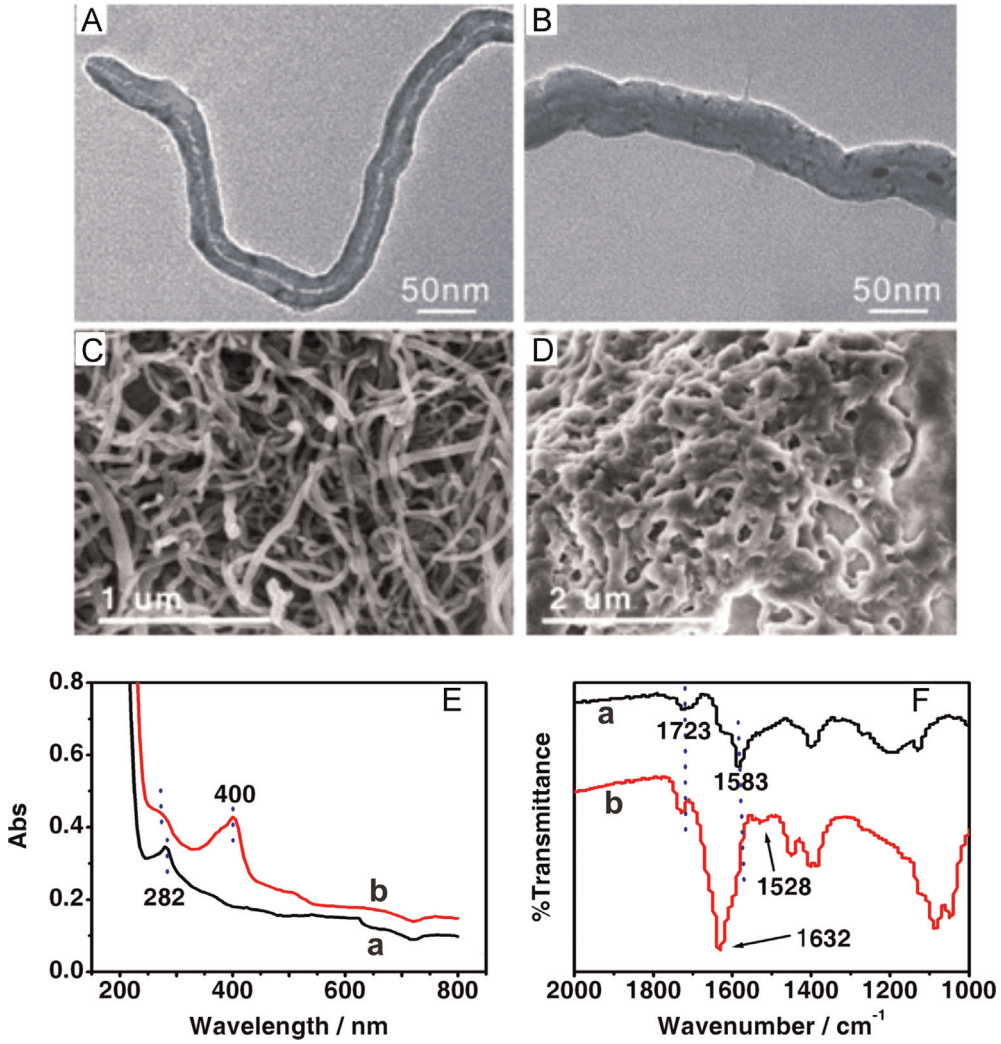

Fig. 3. TEM (A, B) and SEM (C, D) images of MWNTs (A, C) and {Con A–MWNT–HRP} bioconjugates (B, D), UV–vis absorption spectra (E) and FT-IR spectra (F) of MWNTs (a) and the {Con A–MWNT–HRP} bioconjugates (b).

3.2. Characterization of the {Con A–MWNT–HRP} bioconjugates

TEM was used to characterize MWNTs and the {Con A–MWNT–HRP} bioconjugates. As shown in Fig. 3A, MWNTs had an average diameter of 28 nm. The conjugation of Con A and HRP on MWNTs led to a larger average diameter of 47 nm (Fig. 3B). Furthermore, the surface of the {Con A–MWNT–HRP} bioconjugates was much rougher in texture as compared to that of MWNTs. The resulting bioconjugates were found to be stable for two weeks either from TEM images or from the final activity of Con A and HRP. The size expansion of MWNTs was verified by SEM images (Fig. 3C and D).

The {Con A–MWNT–HRP} bioconjugates were also characterized with UV–vis absorption spectra (Fig. 3E). As can been seen, MWNTs exhibited the absorption peak at 282 nm due to the contribution of the carboxyl groups (curve a). When MWNTs were modified with Con A and HRP, the absorption peak at 400 nm appeared, which was derived from HRP (curve b). Compared to MWNTs, the peak at 282 nm blue-shifted slightly and became broadening because of the interaction between MWNTs and Con A. FT-IR spectrum of MWNTs displayed two peaks at 1723 and 1583 cm^{-1} (Fig. 3F, curve a), which could be assigned to the carbonyl stretch mode of COOH and COO^{-}. After Con A and HRP coupling, two new absorption bands corresponding to amide band I (C=O stretching) and II (N–H bending) respectively appeared at 1632 and 1528 cm^{-1} (Fig. 3F, curve b), and the peaks at 1723 and 1583 cm^{-1} attenuated.

3.3. Optimization of the detection conditions

The concentrations of H_2O_2 and QH_2 greatly influenced the performance of the electrochemical enzyme-catalyzed analysis and were optimized by amperometric measurements. The optimal concentrations of H_2O_2 and QH_2 for enzyme-amplified DPV detection were 0.80 mM and 0.20 mM, respectively (Supplementary).

In the competitive assay, the saturated concentration of the {Con A–MWNT–HRP} bioconjugates binding to the thiomannosyl-functionalized biosensor was responsible for signal generation and was optimized by saturation analysis. As shown in Fig. 4A, the DPV peak current increased with increasing the bioconjugate concentration and trended to a steady value after 0.20 μM, indicating that the saturated binding of the bioconjugates to the biosensing surface-confined mannose. Thus, 0.20 μM of the {Con A–MWNT–HRP} bioconjugates was used for the incubation step.

At the optimized concentration of the {Con A–MWNT–HRP} bioconjugates, Fig. 4B shows the dependence of DPV peak current upon incubation time in the absence of cancer cells (a), and in the presence of QGY-7703 (b), LNCaP (c) and A549 (d) at the cell concentration of 1.0×10^2 cells mL^{-1}. With the increasing incubation time, the peak current increased and tended to a plateau at 60 min. Therefore, the incubation time of 60 min was chosen as the optimal time for the specific recognition between Con A and mannose.

3.4. Comparative study on the performance of the biosensor

The performances of the thiomannosyl-functionalized

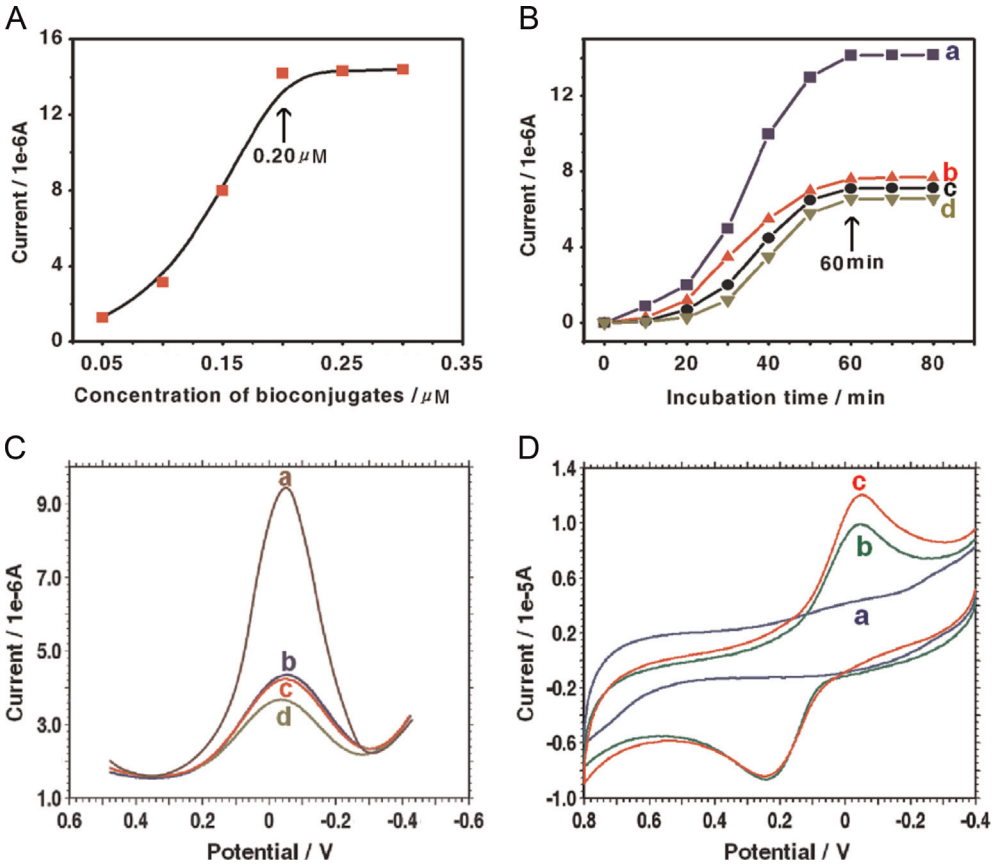

Fig. 4. Dependence of DPV peak current of GCE/MWNT/Au–S–mannose modified with {Con A–MWNT–HRP} upon (A) the bioconjugate concentration and (B) incubation time in the absence of cancer cells (a) and in the presence of QGY-7703 (b), LNCaP (c) and A549 (d) at the cell concentration of 1.0×10^2 cells mL^{-1}. (C) Comparison of DPV curves for the detection of QGY-7703 cells (1.0×10^2 cells mL^{-1}) with the thiomannosyl-functionalized biosensors based on (a) GCE/MWNT/AuNP, (b) GCE/AuNP, (c) bare Au electrode and (d) GCE/MWNT as substrates, respectively. (D) CVs of the GCE/MWNT/Au–S–mannose modified with {Con A–MWNT–HRP} in (a) 10 mM PBS (pH 7.4, containing 0.10 M KCl), (b) PBS containing 0.20 mM QH_2, and (c) PBS containing 0.20 mM QH_2 and 0.80 mM H_2O_2.

biosensor with different substrates (GCE/MWNT/AuNP, GCE/AuNP, bare Au electrode, and GCE/MWNT) were evaluated in the comparative study. Fig. 4C displays DPV peak current for the detection of QGY-7703 cells (1.0×10^2 cells mL^{-1}) using the four biosensors based on enzymatic catalysis. As can be shown, the highest peak current was obtained at the biosensor using GCE/MWNT/AuNP, which was attributed to the favorable electronic properties of the AuNP/MWNT and its high surface area for thiomannosyl dimer assembling. The excellent electrical conductivity of the biosensor could improve the detection limits and reduce the risk of false negative determination at low cell concentrations.

After the thiomannosyl-functionalized biosensor was incubated with the {Con A–MWNT–HRP} bioconjugates and QGY-7703 cells (1.0×10^2 cells mL^{-1}), CVs were used to investigate the electrochemical behavior of the resulting electrode in different solutions (Fig. 4D). As can be shown, the biosensor exhibited a low background current without detectable electrochemical responses in blank PBS (curve a). Upon the addition of QH_2 to PBS, a pair of well-defined redox peaks was observed for the redox of QH_2 on the electrode (curve b). After H_2O_2 was added to the above solution, the reduction peak current significantly increased (curve c), suggesting an obvious electrocatalytic process of the immobilized HRP to the oxidation reaction of QH_2 by H_2O_2.

3.5. Electrochemical detection of cancer cells

Taking into account of the critical requirements for cancer detection with high sensitivity in early diagnosis (Rutherford et al., 2013), we applied the thiomannosyl-functionalized biosensor to detect A549, QGY-7703 and LNCaP cells on the basis of the specific recognition between Con A and cell surface mannose. Under optimal conditions, the DPV peak current for the quantification of QGY-7703 cells is depicted in Fig. 5A. As can be seen, the peak current decreased linearly with the logarithmic value of QGY-7703 cell concentration over the range from 1.0×10^2 to1.0×10^6 cells mL^{-1} with detection limit of 40 cells mL^{-1} ($S/N=3$) (curve a, Fig. 5B). Using the same method, A549 and LNCaP cells were also analyzed and the obtained results are summarized in Table 1. The analytical performance of the proposed biosensor has been compared with those cell-based sensors reported in the literatures (Hu et al., 2008; Gu et al., 2009). Characteristics such as the linear range and detection limit are summarized for all of them in Table S1 (Supplementary). As can be observed, the proposed biosensor exhibited good performance for the detection of cancer cells with broad linear ranges and low detection limits.

In order to demonstrate the enhanced sensitivity caused by the application of the {Con A–MWNT–HRP} bioconjugates, the commercially available {Con A–HRP} was used to replace the bioconjugates for performing the same procedure. As shown in curve b (Fig. 5B), the peak current was proportional to the QGY-7703 concentration from 60 to 6.0×10^5 cells mL^{-1} under the optimal {Con A–HRP} concentration. The change of peak current was very slight upon the increase of cell concentration. The detection sensitivity of the proposed strategy was much higher than that obtained from {Con A–HRP} by comparison between the two slopes, verifying the advantages of the designed {Con A–MWNT–HRP} bioconjugates.

Table 1
Detection results of cancer cells using the amplified electrochemical biosensor.

Cell	A549	QGY-7703	LNCaP
Linear equation	i_p (μA)= $8.85-1.15\lg c$	i_p (μA)= $10.12-1.25\lg c$	i_p(μA)= $9.39-1.14\lg c$
Linear range (cells mL^{-1})	20–4.0×10^5	1.0×10^2–1.0×10^6	40–1.0×10^6
R^2	0.989	0.987	0.988
Detection limit (cells mL^{-1})	10	40	15

The precision and reproducibility of the electrochemical biosensor were evaluated by using the variation coefficients (CVs) of the intra- and inter-assays. The intra-assay precision of the developed strategy was assessed by analyzing four concentration standards of QGY-7703 for five times per run. The CVs of intra-assay with this method were 6.5%, 6.8%, 5.7%, and 6.3% at 5.0×10^3, 1.0×10^4, 5.0×10^4, 1.0×10^5 cells mL^{-1} QGY-7703, respectively. The CVs of inter-assay using five biosensors made at the same electrode with various batches were 6.8%, 7.2%, 5.9%, and 6.7% at 5.0×10^3, 1.0×10^4, 5.0×10^4, 1.0×10^5 cells mL^{-1} QGY-7703, respectively. These results indicated that the precision and reproducibility of the biosensor were acceptable. When the thiomannosyl-functionalized biosensor and the {Con A–MWNT–HRP} bioconjugates were stored in the refrigerator at 4 °C, the peak current was still retained at 90.6% value of the initial response after a storage period of two weeks, showing a quite satisfying stability. Specific recognition of the {Con A–MWNT–HRP} bioconjugates to the biosensing surface-confined mannose was also investigated (Supplementary). The results indicated that the {Con A–MWNT–HRP} bioconjugates exhibited highly specific recognition to the thiomannosyl-functionalized biosensor.

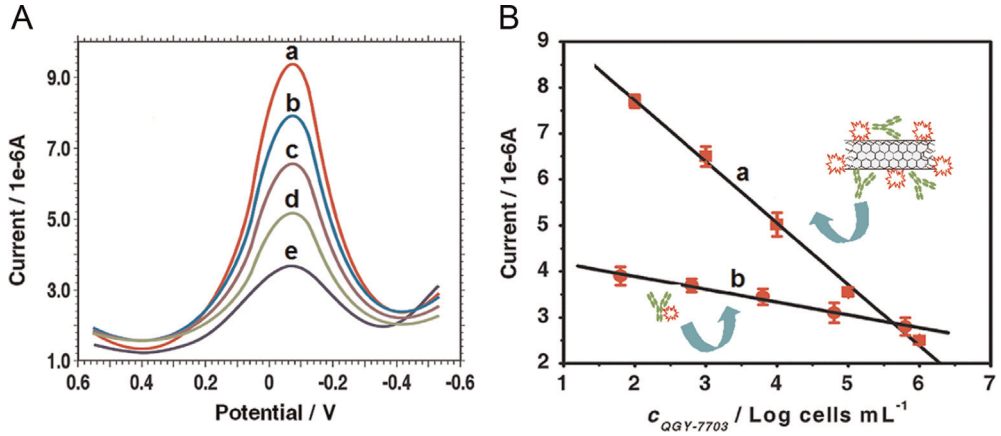

Fig. 5. (A) DPV curves of the thiomannosyl-functionalized electrochemical biosensor obtained with QGY-7703 cell concentrations of 1.0×10^2, 1.0×10^3, 1.0×10^4, 1.0×10^5, 1.0×10^6 cells mL^{-1} (from a to e). (B) Plots of peak current vs logarithm of QGY-7703 cell concentration using (a) the {Con A–MWNT–HRP} and (b) {Con A–HRP} for recognition. The error bars represented the standard deviations calculated from six electrodes.

3.6. Evaluation of mannose expression on cancer cells

In living systems, the glycan expression conveys information about the physiological state of various cancers, which holds great relevance for cancer diagnosis and treatment. Therefore, the sensitive and facile biosensor was applied to the analysis of mannose expression on different cancer cells. To this purpose, mannose sample was first detected by employing the thiomannosyl-functionalized biosensor. As shown in Fig. S4A (Supplementary), the DPV peak current (i_p) is proportional to mannose concentration ($c_{mannose}$) in the ranges of 0.05–1.05 μM (R^2=0.992), which served as the standard curve. The linear regression equation was

$$i_p(\mu A) = 4.98 - 0.68 c_{mannose}(\mu M) \quad (1)$$

Then, the proposed biosensor was applied to detect QGY-7703 cells at different concentrations. Fig. S4B (Supplementary) displays the linear relationship between the peak current (i_p') and QGY-7703 cell concentration ($c_{QGY\text{-}7703}$) ranging from 2.0×10^4 to 4.5×10^4 cells mL^{-1} (R^2=0.991). The linear regression equation was

$$i_p'(\mu A) = 5.06 - 1.73\times10^{-5} c_{QGY-7703} \quad (2)$$

Meanwhile, the obtained i_p' for QGY-7703 cell detection could be converted into the number of mannose according to Eq. (1), which represented mannose expression on QGY-7703 cells. Consequently, with the use of (Eqs. (1) and 2), the amount of mannose on each QGY-7703 cell surface ($n_{mannose}$) could be calculated according to the following equation:

$$n_{mannose} = \frac{(4.98 - i_p)\times10^{-6}\times6.02\times10^{23}}{0.68\times10^3 c_{cell}}$$

where c_{cell} was cell concentration in cells mL^{-1}. Four parallel measurements gave the average amount of mannose on single cell surface to be 1.3×10^{10} molecules for QGY-7703. Using the same method, the number of mannose on each cell surface was also determined to be 5.8×10^{10} molecules for A549 and 1.9×10^{10} molecules for LNCaP, respectively. The mannose expression status on living cell surface detected by the biosensor was in good agreement with the results from Fluorescent Microscopy studies (Supplementary).

4. Conclusions

This work developed a thiomannosyl-functionalized biosensor for signal amplification toward highly sensitive electrochemical detection of mannose expression on cancer cells. Thiomannosyl dimer was synthesized to design the biosensor by direct and rapid one-step protocols. The greatly enhanced sensitivity relies upon a signal-amplification scheme: (1) GCE/MWNT/AuNP was used as the substrate for thiomannosyl dimer assembling, which could increase electrical conductivity and provide large surface area, and (2) MWNTs as the enzyme-loading carriers can load many enzyme molecules on each MWNT. The labeling protocol allows multiple signals per binding event provided by the use of {Con A–MWNT–HRP} bioconjugates in place of conventional {Con A–HRP}. The thiomannosyl-functionalized electrochemical biosensor offers a useful tool for competitive assay of cell surface mannose with high sensitivity, accuracy and rapid response. The proposed strategy can be extended to other glycans and lectin recognition events, and thus provides a promising potential in the analysis of cell surface glycan expression and evaluation of glycan functions during the various steps of tumorigenesis.

Acknowledgments

This work was supported by the National Natural Science Foundation of China (21205051, 21305052 and 21205050), and Project Funded by the Priority Academic Program Development of Jiangsu Higher Education Institutions (1033000006).

Appendix A. Supplementary material

Supplementary data associated with this article can be found in the online version at http://dx.doi.org/10.1016/j.bios.2015.06.051

References

Beitollahi, H., Mazloum-Ardakani, M., Ganipour, B., Naeimi, H., 2008. Biosens. Bioelectron. 24, 362–368.
Bian, S., Zieba, S.B., Morris, W., Han, X., Richter, D.C., Brown, K.A., Mirkin, C.A., Braunschweig, A.B., 2014. Chem. Sci. 5, 2023–2030.
Dai, X., Nekrassova, O., Hyde, M.E., Compton, R.G., 2004. Anal. Chem. 76, 5924–5929.
Dai, Z., Kawde, A.-N., Xiang, Y., La Belle, J.T., Gerlach, J., Bhavanandan, V.P., Joshi, L., Wang, J., 2006. J. Am. Chem. Soc. 128, 10018–10019.
Deng, L., Norberg, O., Uppalapati, S., Yan, M., Ramstrom, O., 2011. Org. Biomol. Chem. 9, 3188–3198.
Ding, L., Cheng, W., Wang, X., Xue, Y., Lei, J., Yin, Y., Ju, H., 2009. Chem. Commun., 7161–7163.
Gorelik, E., Galili, U., Raz, A., 2001. Cancer Metastasis Rev. 20, 245–277.
Gu, M., Zhang, J., Li, Y., Jiang, L., Zhu, J.-J., 2009. Talanta 80, 246–249.
Haslam, S.M., North, S.J., Dell, A., 2006. Curr. Opin. Struct. Biol. 16, 584–591.
Helenius, A., Aebi, M., 2001. Science 291, 2364–2369.
Hollingsworth, M.A., Swanson, B.J., 2004. Nat. Rev. Cancer 4, 45–60.
Hu, H.-L., Jiang, H., Wang, X.-M., Chen, B.-A., 2008. Electrochem. Commun. 10, 1121–1124.
Jeong, B., Akter, R., Han, O.H., Rhee, C.K., Rahman, M.A., 2013. Anal. Chem. 85, 1784–1791.
Karimi-Maleh, H., Tahernejad-Javazmi, F., Ensafi, A.A., Moradi, R., Mallakpour, S., Beitollahi, H., 2014. Biosens. Bioelectron. 60, 1–7.
Lotierzo, M., Abuknesha, R., Davis, F., Tothill, I.E., 2012. Environ. Sci. Technol. 46, 5504–5510.
Lyu, Y.-K., Lim, K.-R., Lee, B.Y., Kim, K.S., Lee, W.-Y., 2008. Chem. Commun. 44, 4771–4773.
Ma, Q., Nakazato, K., 2014. Biosens. Bioelectron. 51, 362–365.
Mader, A., Gruber, K., Castelli, R., Hermann, B.A., Seeberger, P.H., Radler, J.O., Leisner, M., 2012. Nano Lett. 12, 420–423.
Martin, C.E., Broecker, F., Eller, S., Oberli, M.A., Anish, C., Pereira, C.L., Seeberger, P.H., 2013. Chem. Commun. 49, 7159–7161.
Matsumoto, A., Sato, N., Kataoka, K., Miyahara, Y., 2009. J. Am. Chem. Soc. 131, 12022–12023.
Mazloum-Ardakani, M., Beitollahi, H., Amini, M.K., Mirkhalaf, F., Mirjalili, B.-F., 2011. Biosens. Bioelectron. 26, 2102–2106.
Mazloum-Ardakani, M., Taleat, Z., Khoshroo, A., Beitollahi, H., Dehghani, H., 2012. Biosens. Bioelectron. 35, 75–81.
Ohtsubo, K., Marth, J.D., 2006. Cell 126, 855–867.
Park, S., Sung, J.-W., Shin, I., 2009. ACS Chem. Biol., 4; , pp. 699–701.
Peng, Y., Jiang, J., Yu, R., 2014. Anal. Methods 6, 2889–2893.
Pussak, D., Ponader, D., Mosca, S., Ruiz, S.V., Hartmann, L., Schmidt, S., 2013. Angew. Chem. Int. Ed. 52, 6084–6087.
Rutherford, M.J., Hinchliffe, S.R., Abel, G.A., Lyratzopoulos, G., Lambert, P.C., Greenberg, D.C., 2013. Int. J. Cancer 133, 2192–2200.
Scavetta, E., Mazzoni, R., Mariani, F., Margutta, R.G., Bonfiglio, A., Demelas, M., Fiorilli, S., Marzocchi, M., Fraboni, B., 2014. J. Mater. Chem. B 2, 2861–2867.
Seo, J.H., Adachi, K., Lee, B.K., Kang, D.G., Kim, Y.K., Kim, K.R., Lee, H.Y., Kawai, T., Cha, H.J., 2007. Bioconjugate Chem. 18, 2197–2201.
Shin, I., Park, S., Lee, M.R., 2005. Chemistry – Eur. J. 11, 2894–2901.
Singh, A., Park, S., Yang, H., 2013. Anal. Chem. 85, 4863–4868.
Svarovsky, S.A., Joshi, L., 2014. Anal. Methods 6, 3918–3936.
Yamada, K., Hirabayashi, J., Kakehi, K., 2013. Anal. Chem. 85, 3325–3333.
Zhang, X., Geng, P., Liu, H., Teng, Y., Liu, Y., Wang, Q., Zhang, W., Jin, L., Jiang, L., 2009. Biosens. Bioelectron. 24, 2155–2159.
Zhang, X., Lu, W., Han, E., Wang, S., Shen, J., 2014. Electrochim. Acta 141, 384–390.
Zhang, X., Teng, Y., Fu, Y., Xu, L., Zhang, S., He, B., Wang, C., Zhang, W., 2010. Anal. Chem. 82, 9455–9460.
Zhang, X., Teng, Y., Fu, Y., Zhang, S., Wang, T., Wang, C., Jin, L., Zhang, W., 2011. Chem. Sci. 2, 2353–2360.
Zhang, X., Zhang, F., Zhang, H., Shen, J., Han, E., Dong, X., 2015. Talanta 132, 600–605.
Zhao, Y., Liu, L., Kong, D., Kuang, H., Wang, L., Xu, C., 2014. ACS Appl. Mater. Interfaces 6, 21178–21183.
Zheng, T., Zhang, Q., Feng, S., Zhu, J.-J., Wang, Q., Wang, H., 2014. J. Am. Chem. Sci.

136, 2288–2291.
Zou, L., Pang, H.-L., Chan, P.-H., Huang, Z.-S., Gu, L.-Q., Wong, K.-Y., 2008. Carbohydr. Res. 343, 2932–2938.